



RESEARCH ARTICLE

Correlation between the number of interstitial neurons of the white matter and number of neurons within cortical layers: Histological analyses in postnatal macaque

Bashir Ahmed¹  | Alvaro Duque² | Pasko Rakic² | Zoltán Molnár¹ 

¹Department of Physiology, Anatomy and Genetics, Sherrington Building, University of Oxford, Oxford, UK

²Department of Neuroscience, Yale University School of Medicine, New Haven, Connecticut, USA

Correspondence

Bashir Ahmed and Zoltán Molnár, Department of Physiology, Anatomy and Genetics, Sherrington Building, University of Oxford, Oxford, UK.

Email: bashir.ahmed@dpag.ox.ac.uk and zoltan.molnar@dpag.ox.ac.uk

Funding information

National Institutes of Health, Grant/Award Number: MH113257; Biotechnology and Biological Sciences Research Council, Grant/Award Number: (UK) BB/X008711/1; Einstein Stiftung Berlin; MRC (UK), Grant/Award Number: MR/W029073/1

Abstract

We have examined the number and distribution of NeuN-immunoreactive cortical white matter interstitial cells (WMICs) and compared them to the neurons in layers 1–6 across the overlying cortex in coronal sections from postnatal macaques. The data have been gathered from over 300 selected regions at gyral crowns, at sulci, and at linear regions of the cortex where we also determined cortical layer thicknesses: standard thicknesses and tangential thicknesses. Cortical thicknesses and cell numbers showed variability according to gyral, linear, or sulcal regions. In spite of these variations, our standardized cell numbers in layers 1 to 6b and interstitial cells underlying layer 6b-white matter boundary have shown a consistent correlation between the number of WMICs and the number of layer 5 and 6a cortical neurons on all cortical regions studied: for each WMIC, there are on the order of five cortical neurons in layer 5 and approximately three cortical neurons in layer 6a, irrespective of the origins of the selected cortical area or whether they are from gyral, linear, or sulcal regions. We propose that the number of interstitial neurons in the postnatal macaque cortex is correlated to the density of neurons within layers 5 and 6a and, from a clinical perspective, the change in density or distribution of interstitial neurons in schizophrenia or epilepsy may in fact be linked to the number of layers 5 and 6a neurons.

KEYWORDS

cortical layer thickness, gyral linear and sulcal regions, NeuN-labeled cells, neuronal cell densities, QuPath: Open-source software (RRID:SCR_018257)

1 | INTRODUCTION

Interstitial neurons of the cerebral cortical white matter (WMICs) are heterogeneously distributed within the entire cortical white matter and in number form approximately 3%–5% of all cortical neurons (Mortazavi et al., 2016, 2017; Sedmak & Judaš, 2019, 2021; Swiegers et al., 2019, 2021). The segmentation of the white matter has been described

by classical anatomical literature (Brodman, 1914; Sachs, 1892; Von Monakow, 1905), and WMICs that are situated in the distal segment of white matter are known to be the remnants of neurons found within the subplate (Chun & Shatz, 1989; Kostović & Rakic, 1980, 1990; Kostović et al., 2014; Valverde & Facal-Valverde, 1988; Žunić Išasegi et al., 2018) and during development undergo cell death such that in the adult only 20% survive (Chun & Shatz, 1989; Duque et al., 2016). During

This is an open access article under the terms of the [Creative Commons Attribution](https://creativecommons.org/licenses/by/4.0/) License, which permits use, distribution and reproduction in any medium, provided the original work is properly cited.

© 2024 The Author(s). The *Journal of Comparative Neurology* published by Wiley Periodicals LLC.

development subplate neurons are the first to form synapses within the subplate zone. They were described by Kostović et al. (1973) in the fetal dog and Kostović and Molliver (1974) in human. The first synapses onto interstitial neurons of the cortical white matter of postnatal monkey were first described using rapid Golgi impregnations, by acetylcholinesterase histochemistry and by electron microscopy in a study by Kostović and Rakic (1980), who determined subplate origin by birth dating with [^3H]thymidine ([^3H]TdR) autoradiography. The function of deep synapses was documented by electrophysiological recording in the newborn dog by Molliver and Van der Loos (1970). Subsequently, these synapses were further analyzed with optic radiation stimulation in brain slices from developing cats using current source density analysis (Friauf & Shatz, 1991; Friauf et al., 1990); in rat and mouse using direct thalamic stimulation in thalamocortical slices combined either with current source density analysis (Molnár et al., 2003) or with an optical recording of voltage-sensitive dyes and patch clamp recordings (Higashi et al., 2002, 2005). The subplate neurons have been found to be essential in directing thalamic fibers to generate functional circuitry in cortical cells as damage or alteration to the subplate or the subplate pathways results in modifications of connections (Ghosh et al., 1990; Kanold & Luhmann, 2010; Kanold & Shatz, 2006; Kostović & Rakic, 1990; López-Bendito & Molnár, 2003).

Because of the early birthdate and shared gene expressions with sauropsids, the subplate neurons and their remnants in the adult brain are generally considered to be the derivatives of phylogenetically an old system (Das & Kreutzberg, 1968; Juan et al., 2011; Judaš et al., 2010; Kostović et al., 2011; Marin-Padilla, 1971; Wang et al., 2011). However, the novel and largely expanded populations of subplate in the primate might suggest that some of the subplate neurons have novel origin and novel functions in the developing and in the adult primate brain (Montiel et al., 2011).

In the adult, WMICs form a diverse population both neurochemically and morphologically (Feldmeyer, 2023). They express a range of neuronal identities: glutamatergic, GABAergic, peptidergic, and nitrinergic (Chan-Palay et al., 1985; Fischer & Kuljis, 1994; Judaš et al., 1999; Kostović et al., 1991; Smiley et al., 1998). All WMICs are immuno-positive for the neuronal marker NeuN (Garcia-Marin et al., 2010; Sedmak & Judaš, 2019). They have diverse and extensive dendritic arborization patterns: are mono-to-multi tufted cells, are multipolar cells, and can be either inverted pyramidal or pyramidal cells (Berman & Fredrickson, 1992; Judaš et al., 2010; Meyer et al., 1992; Uylings & Delalle, 1997; Garcia-Marin et al., 2010). GABAergic cells form synaptic connections locally on other WMICs (Torres-Reveron & Friedlander, 2007), and nitrinergic cells have axons opposed to blood vessels (Regidor, Edvinsson & Divac, 1993; Judaš et al., 2010), whereas glutamatergic cells send axons subcortically and cortically (Clancy & Cauller, 1999; Clancy et al., 2001; Hoerder-Suabedissen et al., 2018; Meyer et al., 1991; Okhotin & Kalinichenko, 2003; Shering & Lowenstein, 1994; Viswanathan et al., 2017). Electrophysiological recordings from WMICs show reciprocal connections with cortical layers 5 and 6 (Hanganu et al., 2002; Zolnik et al., 2023).

Interstitial cells have been implicated in sleep regulation (Kilduff et al., 2011) and pathology, especially schizophrenia and epilepsy, where an increased density of interstitial neurons has been observed

(Akbarian et al., 1996; Anderson et al., 1996; Eastwood & Harrison, 2003, 2005; Fung et al., 2014; Kirkpatrick et al., 1999, 2003; Meencke, 1983; Richter et al., 2016).

The distribution of interstitial neurons within the white matter is not uniform, the highest density is around gyral crowns, and the lowest density is at sulcal regions (Garcia-Marin et al., 2010; Rojiani et al., 1996; Sedmak & Judaš, 2019; Swiegers et al., 2021). In addition, the infragranular layers also vary such that they are thickest at gyri and thinnest at sulci, whereas layer 1 is thickest at sulci (Horiuchi-Hirose & Sawada, 2016). These facts taken together with the known WMIC synaptic connections to layer 1 (Clancy & Cauller, 1999; Meyer et al., 1991) and reciprocal connections to layers 5 and 6 implied a neuronal relationship between interstitial cells and the overlying cortical cells.

We, therefore, decided to investigate whether such a relationship existed between the variation of cell density of WMICs at gyral, linear, and sulcal regions with the concomitant variation in the overlying thicknesses and cell densities of the cortical layers at these regions across seven coronal sections, approximately 1 cm apart, from anterior to posterior of the right hemisphere in three postnatal macaques.

2 | METHODS

The entire study has been undertaken on archived material, without the need to sacrifice any (new) animals, and is based on publicly available materials in Collection 6 of the MacBrain Resource Center hosted in the Department of Neuroscience at Yale University School of Medicine (<https://medicine.yale.edu/neuroscience/macbrain/>). Details of histological and immunostaining of tissue have been published (Duque et al., 2007, 2013; Rash et al., 2019).

We have examined high-quality images obtained at x20 of histological sections of NeuN immuno-labeled neurons from three macaques: a female of postnatal day 7 (B64p7, brain weight 53.42 g), a male 1.01-year old (B87y1, brain weight 96.9 g), and a female 8.07-year old (B72y8, brain weight 80.13 g). The distributions of labeled neurons in the images were detected by the image analysis software QuPath [Bankhead et al., 2017. QuPath: Open-source software for digital pathology image analysis. Scientific Reports 7, 16878.—<https://doi.org/10.1038/s41598-017-17204-5>, RRID:SCR_018257]. QuPath is an open-source image analysis software and provides a readymade script for the detection of cells and a range of parameters that can be modified for best results. The data of the detected cells are comprehensive and are made available as a text-based spreadsheet that can be analyzed in detail. We have analyzed seven coronal sections (Figure 1, 50 μm thick), approximately 1 cm apart, from anterior to posterior of the right hemisphere of the three macaques (Figure 1a is for B64P7; Figure 1b for B87y1, and Figure 1c for B72y8), and quantified neuronal numbers in layers 1 to 6b and the underlying interstitial cells of the white matter in three regions of the cortex: linear (unfolded cortex with parallel laminae), sulcal, and gyral. The laminae boundaries were defined by visual inspection across the cortical depth and based on marked cell density changes in the NeuN-labeled sections and in some cases with the aid of adjacent Nissl-stained sections (Figure 2). We excluded cases where laminar boundaries across the

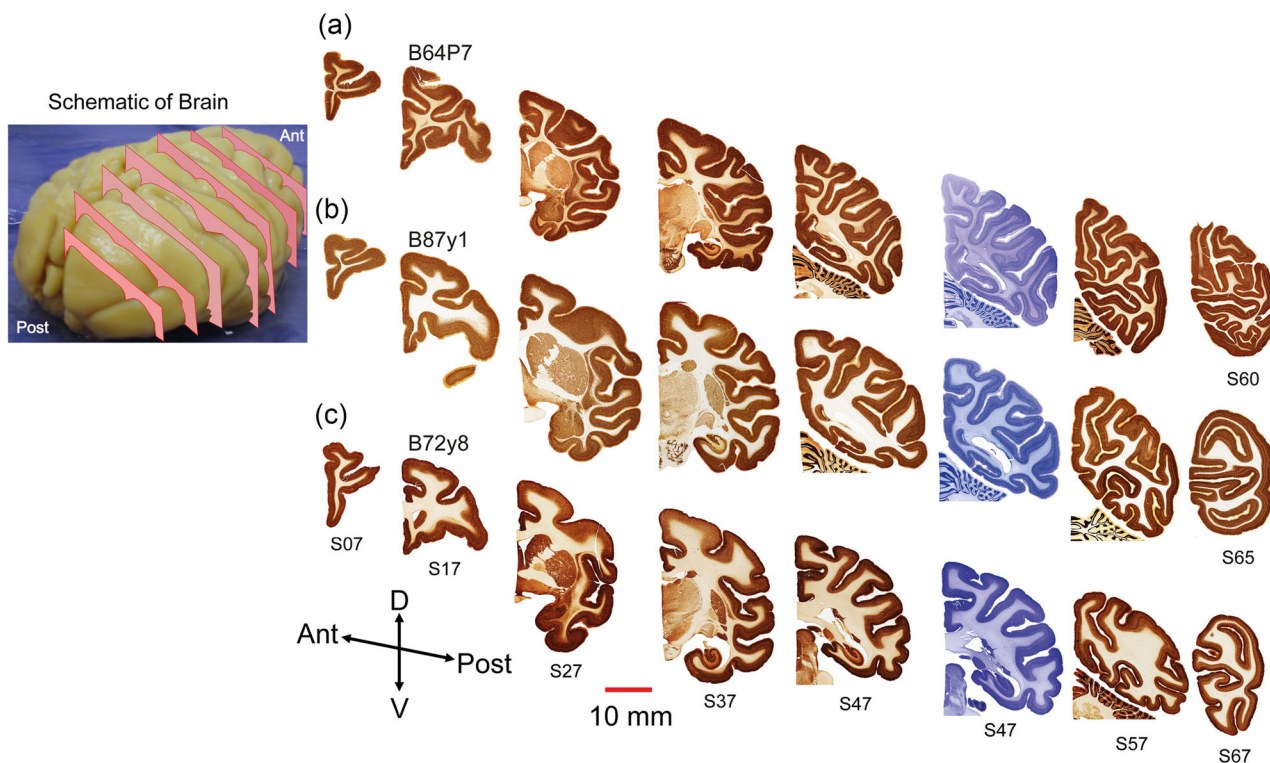


FIGURE 1 Coronal sections analyzed from three macaques: a postnatal 7 day old (B64P7, a), a 1.01-year old (B87y1, b) and an 8.07-year old (B72y8, c). The sections were NeuN immunolabelled with each section 50 μ m in thickness and approximately 1 cm apart, as shown in the right hemisphere from the schematic of a macaque brain. Adjacent Nissl sections (S47) are also shown.

TABLE 1 Total gyri, linear regions, and sulci analyzed in the three macaques (124; 84; 100 = 308 selected regions).

Macaque ID	Gyri	Linear	Sulci
B64P7	37	25	33
B87y1	46	36	32
B72y8	41	23	35

cortical depth could not be clearly defined. The boundary between layer6b and white matter was initially specified under QuPath by a sharp fall in cell density (Figure 2; blue line in insets (b)) and then defined by visual inspection to exclude the presence of pyramidal cells or clusters of pyramidal cells within the white matter (Figure 2; green line in insets(b)).

Table 1 shows the total number of gyri, linear regions, and sulci analyzed in the three macaques.

We have applied a protocol as shown in Figure 3 to determine a standardized number of cells detected over a 100 μ m length and within the thickness of the cortical layers in cortical regions located at gyri, linear, and sulci. For a layer, where the cortical layer thickness varied, we measured the thickness every 100 μ m along the dorsal border and then determined a standard thickness (St) as determined in Figure 3a, for layer 5. We did this in all layers where the thickness along the layer substantially varied. In other layers, where the thickness remained relatively constant, we determined the standardized thickness by dividing

the layer area by the mean length of the dorsal and ventral borders defining the layer. This was the case for all layers from the linear regions, layers 1, 2, and 4 from gyri, and layers 2, 4, 6a, and 6b from sulci. In a few cases, layers 3 and 5 were also relatively constant in thickness, and their thicknesses were also determined in this manner. In addition, we measured the thickness of layers tangentially (tangential thickness [Tt]) from the pial surface to the white matter across the gyral crown, across the sulci, and across the middle of the linear regions. The details of these measurements are given in Figure 4.

The examples in Figure 4 show how the layer thicknesses were determined at gyral (Figure 4a), sulcal (Figure 4b), and linear (Figure 4c) regions. The inset (a, Figure 4a-c) shows the measurement of the Tt and inset (b, Figure 4a-c) follows the protocol shown in Figure 3a to determine the mean thickness of the layer by measuring the thickness across the layer at a range of separations. The graphs on the right in each case show the resultant mean thicknesses at each separation. In addition, on the left of the graph are the Tt values (Tt, green dot), and the St values determined by dividing the area of the respective layer by the mean of the dorsal and ventral boundaries of the layer (St, blue dot). For layers that remained approximately constant along their length, this thickness value was taken as the St (Figure 4c). Where the layer thicknesses varied along their length, the St value was the mean thickness calculated at 100 μ m separations (Figure 4a,b).

For obtaining the standard cell numbers for WMICs at gyral, linear, and sulcal regions, we determined a thickness based on its area divided by the length of the perimeter along the layer 6b-white matter border

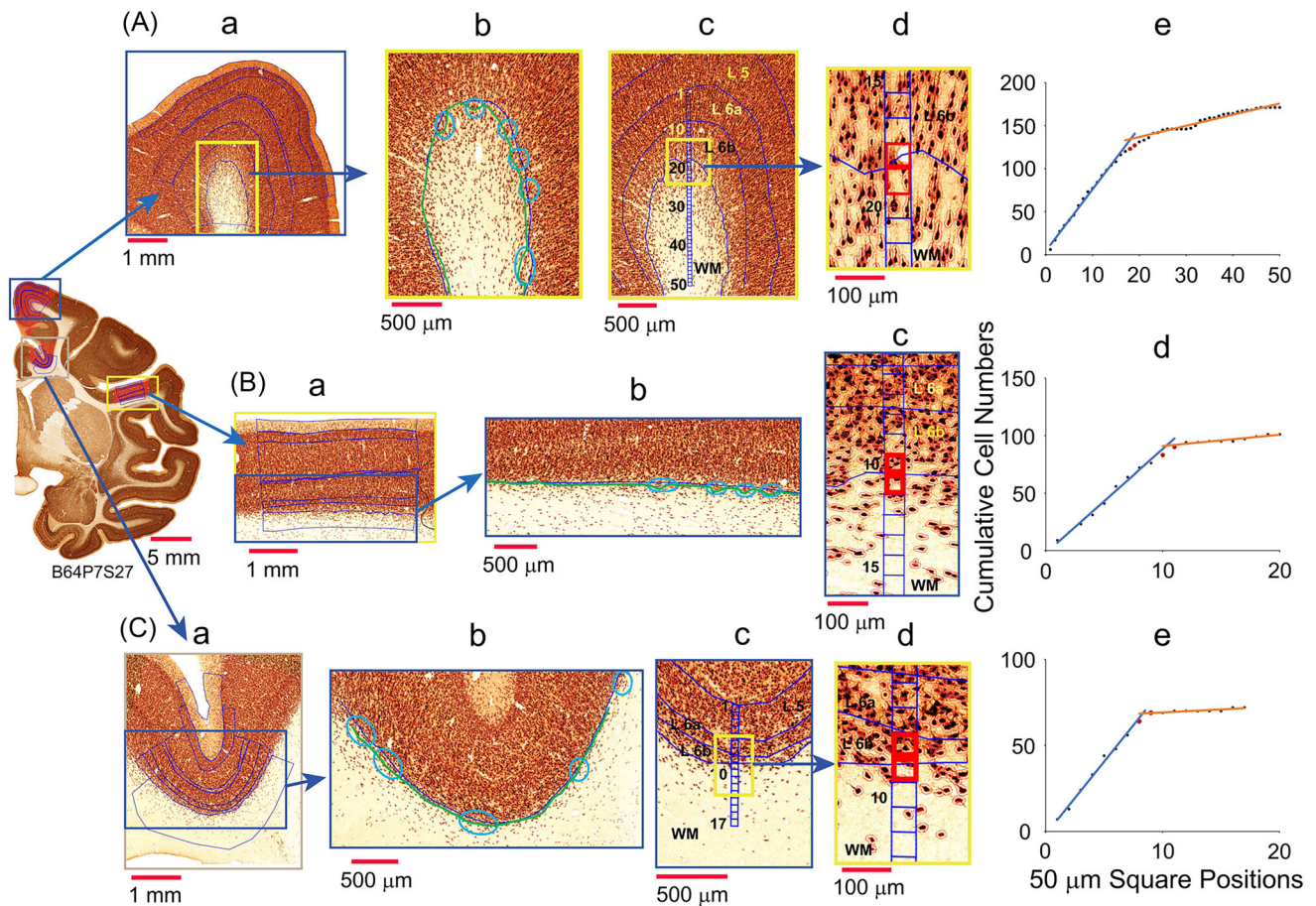


FIGURE 2 Determination of the layer 6b and white matter border at gyral (a), linear (b), and sulcal (c) regions. The blue line in insets (b) was defined as the border between layer 6b and the white matter and was based on density change determined by eye. Further inspection of this region revealed clumps of cells, highlighted as light blue areas in inset (b). The border was then redefined around these neuronal clumps (green line). Insets (c and d) show the outlines of the determined layer 6b white matter boundary with two 50 μ m squares highlighted in red. The graphs (e, d, and e) plot the cell numbers in the 50 μ m squares as accumulated cell numbers versus position of the squares running from cortical layers to the white matter. The linearly fitted lines (for cells numbers within cortical layers in blue and for cells within white matter in orange) intersect at 50 μ m squares shown as red dots. These squares are highlighted in red in insets (d, c, and d).

(Figure 3b). The product of this St with the cell density and a length of 100 μ m defined our standardized cell numbers.

3 | RESULTS

We have examined the distribution of interstitial cells within the white matter juxtaposed to the layer 6b boundary and the distribution of neurons in layers 1–6 across the overlying cortex in seven NeuN-immunostained serial coronal sections. The data have been gathered at gyral crowns, at sulci, and at linear regions (respectively, 124; 100; 84; = 308 selected regions, see Table 1) of the cortex where we also determined cortical layer thicknesses: St and Tt.

In Figure 5, we show the distribution of layer thicknesses across gyral, linear, and sulcal regions. The upper figures (Figure 5a) are the values of the Standard mean thicknesses, and the lower figures (Figure 5b) are for the Tts. The values in Figure 5a–c are for regions outside primary visual cortex (V1), whereas Figure 5d is combined values

of layer thicknesses across the three macaques for regions within V1. The measurements in Figure 5a–c show that for gyral and linear regions, the supragranular layers (layers 1–4) remain approximately constant in thickness, whereas at the sulcal region, layer 1 substantially thickens (combined St of layer 1 at gyral and linear region $167.8 \pm 3.4 \mu$ m, and at sulcal region $247.0 \pm 7.3 \mu$ m, $p < .01$; combined Tt of layer 1 at gyral and linear region $182.3 \pm 3.6 \mu$ m, and at sulcal region $418.0 \pm 15.8 \mu$ m, $p < .01$), and layer 3 to significantly decrease in thickness (combined St of layer 3 at gyral and linear region $582.1 \pm 12.8 \mu$ m, and at sulcal region $421.5 \pm 13.2 \mu$ m, $p < .01$; combined Tt of layer 3 at gyral and linear region $627.7 \pm 13.9 \mu$ m, and at sulcal region $387.6 \pm 19.4 \mu$ m, $p < .01$).

For the infragranular layers, layers 5, 6a, and 6b in Figure 5a–c, at gyri the layers are thickest, and their thickness decreases such that the sulcal layers are the thinnest (Table 2). For example, layer 6b St declines from its thickest at gyri of $356 \pm 14.0 \mu$ m to its thinnest at sulci of $79.7 \pm 3.4 \mu$ m. Our analyses of layer thicknesses within the primary visual cortical regions (V1) show that layers 3 and 4 are thickest

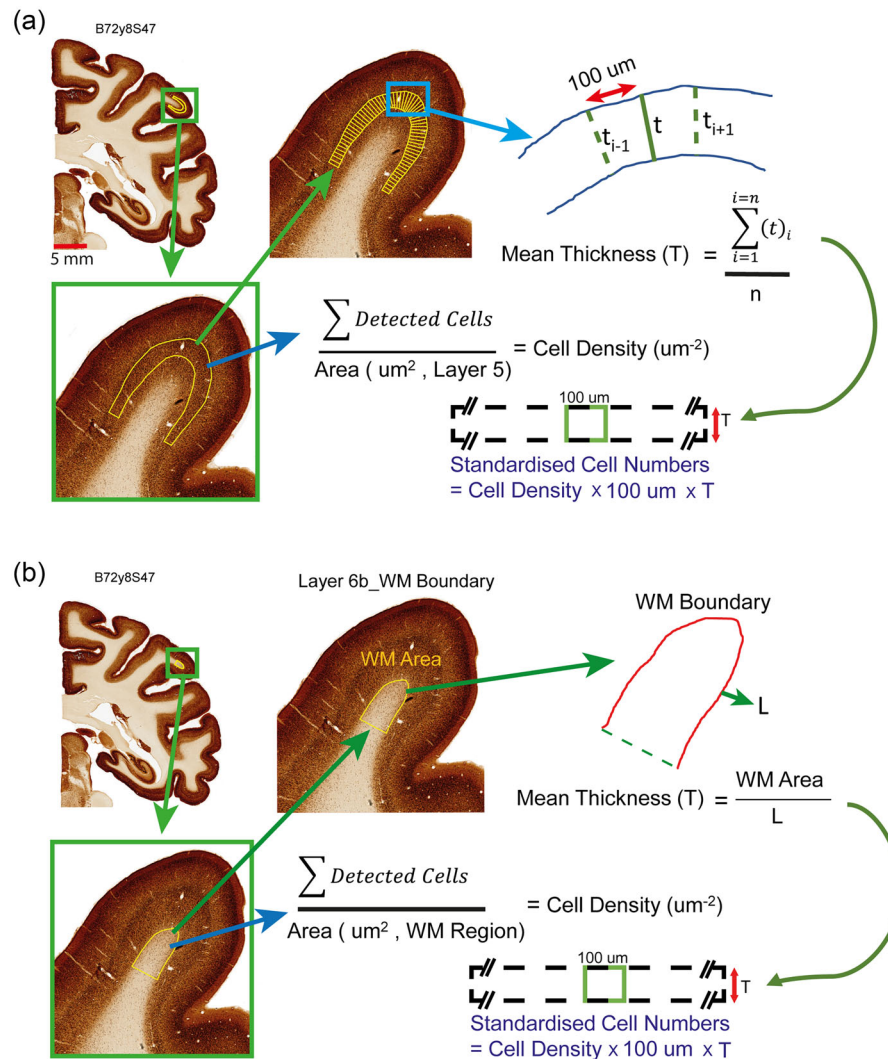


FIGURE 3 Protocol for standardizing layer thicknesses and cell numbers for cortical layers (a), and for interstitial cell of the white matter (b). (a) is an example for layer 5 at a gyral location (B72y8S47) where the layer thickness substantially varied along the length of the layer. In this and similar cases, we measured the thickness of the layer every 100 μm along its dorsal border and then took the average value as the standard thickness (T). In cases where the layer thickness remained fairly uniform along the length of the layer, we defined the standard thickness in these cases as the area divided by the mean of the dorsal and ventral border. We define the standard cell number as the number of cells over 100 μm length of the layer from the product of cell density and standard thickness of the layer (a). For the interstitial cells, we defined the standard thickness (T) by dividing the defined area by the length of the layer 6b—white matter boundary (b). The standardized cell numbers were then defined similarly to a.

TABLE 2 Combined layer thicknesses at gyri, at linear regions, and at sulci in the three macaques in 308 selected regions (124; 84; 100).

Layers	Standard thickness (μm; ± 1 SEM)			Tangential thickness (μm; ± 1 SEM)		
	Gyral	Linear	Sulcal	Gyral	Linear	Sulcal
1	157.1 ± 3.6	186.0 ± 6.8	247.0 ± 7.3	173.6 ± 4.1	197.2 ± 7.0	418.0 ± 15.8
2	172.0 ± 4.0	175.5 ± 5.7	189.3 ± 5.2	187.0 ± 5.2	179.7 ± 6.7	234.4 ± 10.4
3	558.9 ± 16.9	621.2 ± 18.1	421.5 ± 13.2	617.3 ± 19.1	628.5 ± 19.1	387.6 ± 19.4
4	141.7 ± 4.7	127.5 ± 7.3	92.7 ± 4.8	175.9 ± 8.5	128.2 ± 8.1	92.6 ± 6.0
5	377.0 ± 11.8	313.9 ± 14.3	178.1 ± 6.3	527.4 ± 17.9	313.1 ± 14.4	74.7 ± 3.7
6a	236.1 ± 9.7	149.9 ± 6.2	79.7 ± 3.4	356.3 ± 14.0	154.0 ± 7.5	164.3 ± 7.4
6b	234.5 ± 12.6	99.3 ± 7.6	45.5 ± 2.6	442.4 ± 22.0	105.9 ± 9.2	43.1 ± 2.6

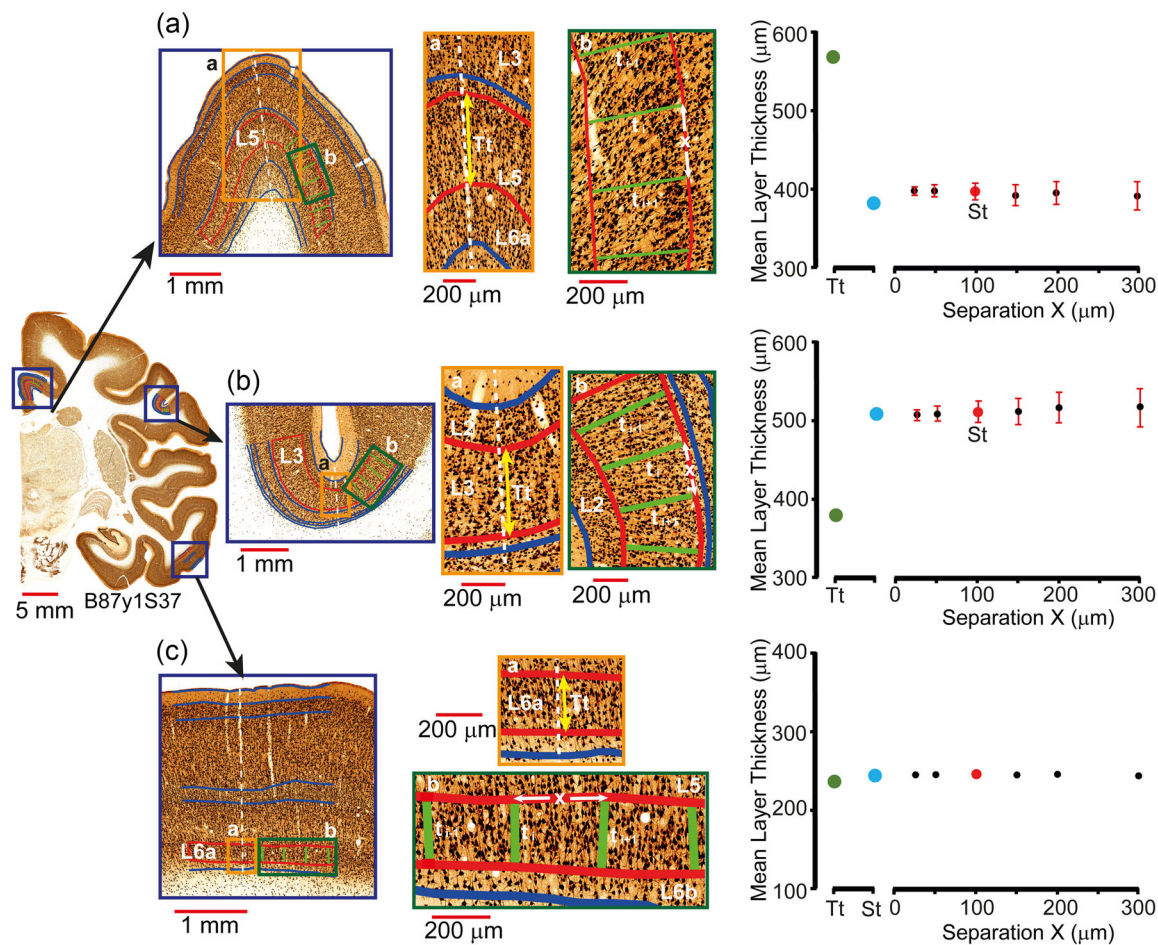


FIGURE 4 Determination of layer thicknesses with examples at gyral (a), sulcal (b), and linear (c) regions. In each example, inset (a) shows the measurement of the tangential thickness (Tt) and inset (b) follows the protocol shown in Figure 3a. The graph on the right in each case shows the resultant thickness values determined at separations (x) of 25, 50, 100, 150, 200, and 300 μm following the protocol (Figure 3a). Error bars are ± 1 SEM. On the left of the graph are the tangential thickness values (Tt, green dot), and the thickness values determined by dividing the area of the layer (highlighted in red: layer 5 in A, layer 3 in B, and layer 6a in c) by the mean of the dorsal and ventral boundaries of the layer (blue dot). In (a) and (b), the thicknesses varied across the respective layer and the standard thickness (St) was taken as the values at 100 μm separation (red dot). For c, layer 6a thickness was approximately uniform, and the value shown as the blue dot was taken as the St. The calculated thicknesses at differing x μm values agreed with this St value. For this graph (c), the error bars were smaller than the size of the black and red dots.

at linear regions of the cortex, and layer 1 is thickest at the sulci. For the infragranular layers, the trend of changes in thickness from gyri to the linear regions is not so evident but the sulcal region still has the thinnest layers, especially layer 6b which is a few cells thick.

In Figure 6, we show the distribution of cell numbers calculated over 100 μm length of the layer and the layer thickness (standardized cell numbers; upper histograms, Figure 6a) and the cell numbers as a ratio to the cell numbers of WMICs (lower histograms, Figure 6b) for sections 47 from the three macaques (Figure 6a-c).

The positions of the gyri, linear, sulci, and WMIC regions are shown in the respective sections in Figure 6. For the supragranular layers, the cell numbers across the gyral, linear, and sulcal regions were found to be variable across the three sections (Figure 6a). However, layers 1 and 2 had the highest cell numbers in the sulcal region. For the infragranular layers and WMICs, there is a systematic decline in cell numbers as we progress from regions gyral to linear to sulcal. This systematic decline in cell numbers for layers 5, 6a, and 6b is matched by the

decline in thickness of these layers (Figure 5a-c). In Figure 6b (lower histograms, Figure 6a-c), we show the ratio between the standardized cell numbers determined at the layers to those determined at WMICs (Figure 6b, IC). For the supragranular layers 1, 2, and 3, we find a systematic increase in the cell ratio progressing from gyral to linear to sulcal with layer 4 showing some variability. For the infragranular layers 6a and 6b, across the three sections, there is variability in this ratio. However, for layer 5, the ratio remains close to 5 (B64P7S47: gyral ($n = 6$, 5.2 ± 0.3), linear ($n = 6$, 5.6 ± 0.5), sulcal ($n = 6$, 5.1 ± 0.3); B87y1S47: gyral ($n = 10$, 5.5 ± 0.4), linear ($n = 7$, 5.1 ± 0.2), sulcal ($n = 7$, 5.6 ± 0.3); B72y8S47: gyral ($n = 8$, 5.0 ± 0.4), linear ($n = 3$, 4.7 ± 0.4), sulcal ($n = 6$, 4.5 ± 0.2), and statistical analysis shows this to be nonsignificant between the three regions and across the three macaques (ANOVA, $p > .43$). This can be interpreted as approximately five neurons of layer 5 to one neuron of WMIC across all three regions and across all three macaques with different postnatal ages.

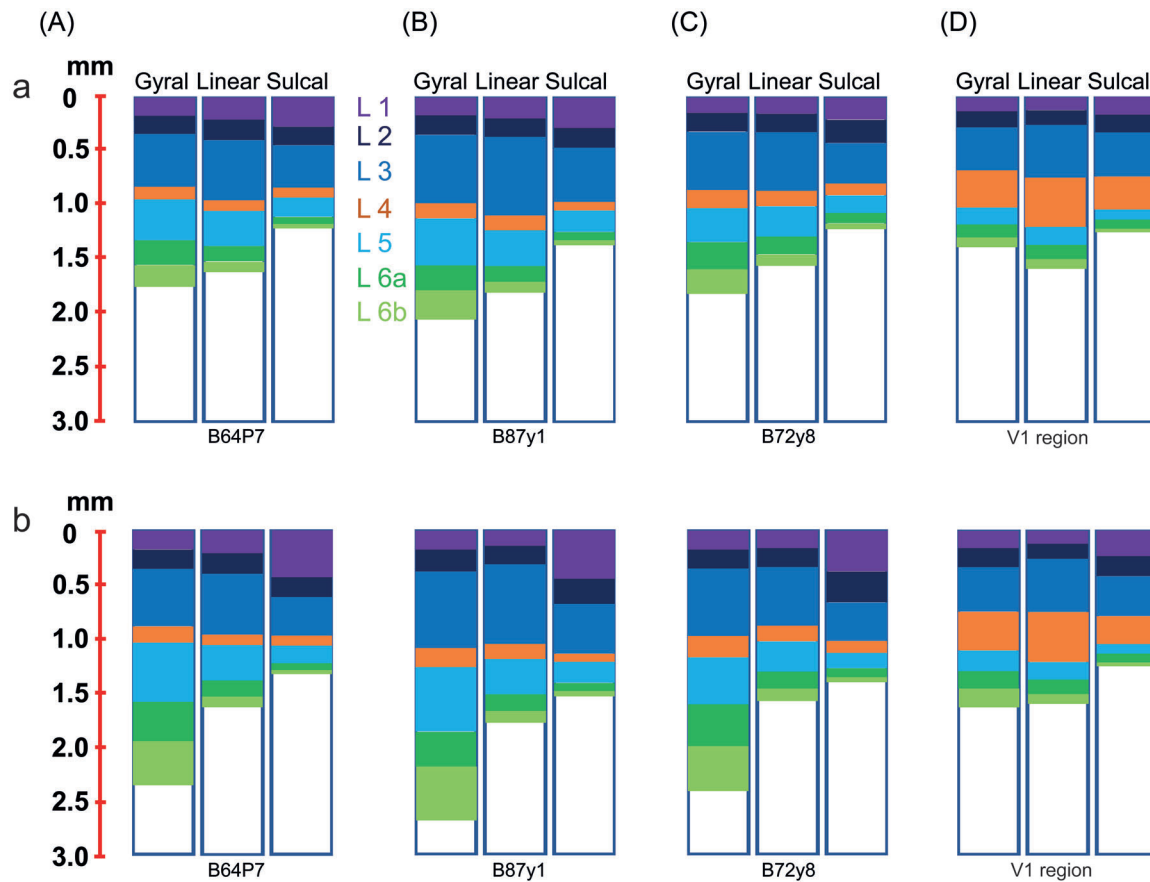


FIGURE 5 Thicknesses of layers 1–6b for the three macaques according to gyral, linear, or sulcal regions in the three different brains (B64P7; B87y1; B72y8). Upper (a) are the standard thicknesses, and the lower figures (b) are for the tangential thicknesses. We show the layer thicknesses separately at gyral, linear, and sulci regions and separately for the macaques (A–C), and for data excluding the primary visual cortex (V1 region). The results show a substantial increase in thickness of layer 1 at sulci compared to gyral and linear regions, whereas layers 3, 4, 5, 6a, and 6b substantially decreased in thickness at sulci. In addition, layers 4, 5, 6a, and 6b showed a systematic decline in thickness from gyral to linear to sulcal for both the standard and the tangential thicknesses. (d) is data collected within the V1 region and is combined across the three macaques. Within V1, layer 1 is increased in thickness at sulci, and layers 3 and 4 are thicker within the linear regions. Layers 5, 6a, and 6b are thinnest at sulcal regions.

TABLE 3 Standardized cell number distributions from gyral, linear, and sulcal regions of interstitial cells of the white matter at anterior, central, and posterior brain regions. Error bars ± 1 SEM.

Right hemisphere brain regions	All coronal sections	Standardized cell numbers for WMICs across the regions from the three macaques		
		Gyral	Linear	Sulcal
Anterior	S7, S17, S27	31.9 \pm 1.5	34.1 \pm 3.8	16.8 \pm 1.1
Central	S37, S47	31.0 \pm 1.7	26.1 \pm 2.2	16.6 \pm 1.0
Posterior	S57, S60, S65, S67	27.9 \pm 1.5	23.0 \pm 2.6	11.4 \pm 0.7
Statistics	Analyses of variance	$p > .18$	$p < .03$	$p < .01$

Abbreviation: WMICs, white matter interstitial cells.

To investigate whether there is any differential distribution of interstitial cells across anterior to posterior cortical regions, we compared the standard cell numbers of coronal sections representing anterior (S07, S17, and S27), central (S37 and S47), and posterior (S57, S60,

S65, S67) cortical regions, and separately at gyri, linear, and sulci. These data were combined across the three macaques (see Table 3). For gyral data, the results were statistically nonsignificant (ANOVA, $p > .18$). For linear data, they were nonsignificant across anterior and central

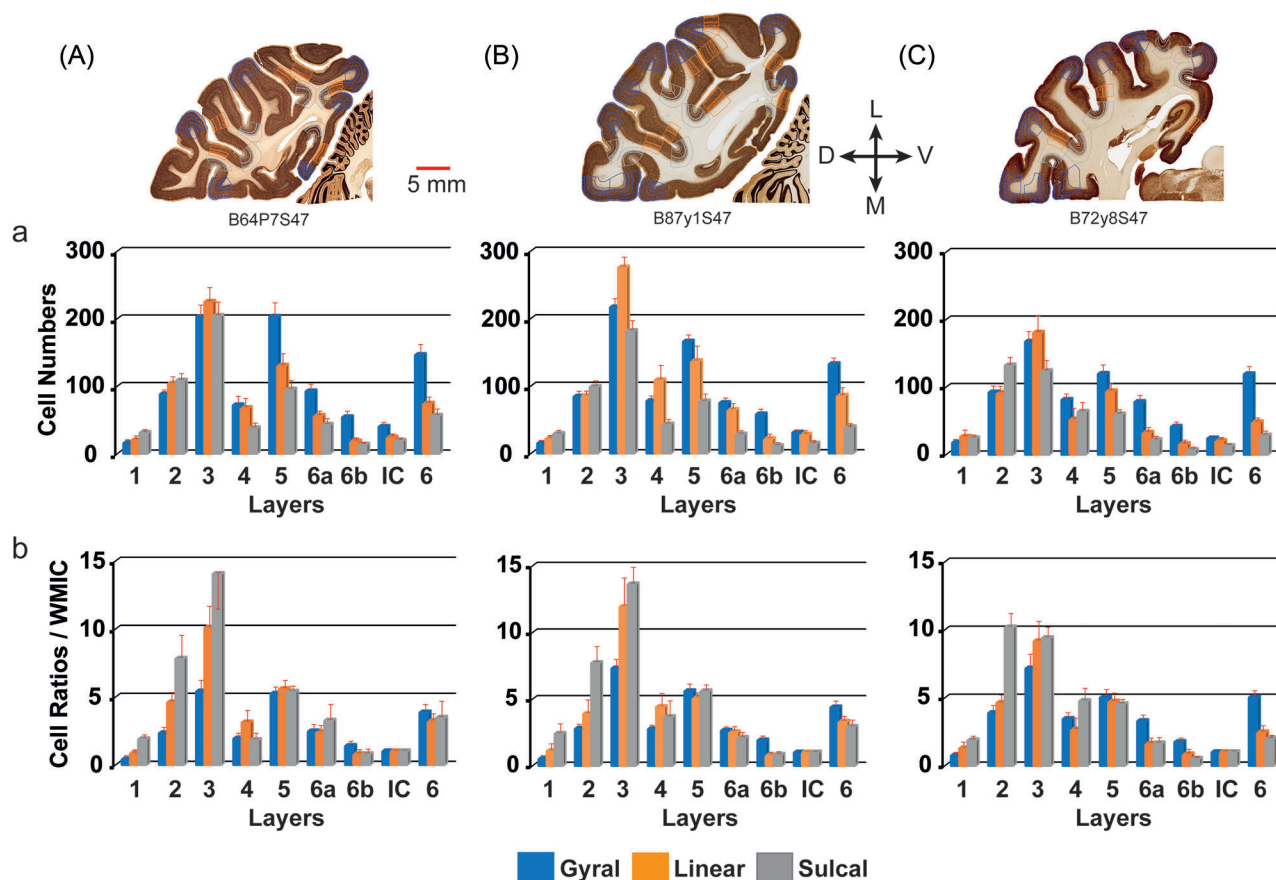


FIGURE 6 Analyses of standard cell numbers and cell numbers per white matter interstitial cell (WMIC) in cortical layers 1–6b and WMIC areas (IC), and combined histogram data for layers 6a and 6b as layer 6. Data from section 47 for postnatal day 7 (B64P7S47, a), for the 1.01-year old (B87y1S47, b), and for 8.07-year old (B72y8S47, c) with gyral, linear regions, and sulci highlighted in the respective coronal sections. The upper histograms are standard cell numbers (a), and the lower histograms (b) are the cell ratios per WMIC. Error bars are ± 1 SEM.

(t -test, $p > .08$), and across central and posterior (t -test, $p > .36$) cortical regions but significantly different between anterior and posterior (t -test, $p < .02$). For the sulcal data, the anterior and central cortical regions were significantly different from the posterior cortical region (t -test, anterior vs. posterior, $p < .01$; central vs. posterior, $p < .01$).

In Figure 7, we show the distribution of cell numbers calculated over 100 μ m length of the layer and the layer thickness (standardized cell numbers; upper histograms, Figure 7a) and the cell numbers as a ratio to the cell numbers of WMICs (lower histograms, Figure 7b) for all seven coronal sections from the three macaques (Figure 7a–c). The standardized cell numbers for supragranular layers 1, 2, and 4 (Figure 7a) show variability but remain approximately invariant across the differing ages from postnatal day 7 (B64P7) to the 8.07-year-old macaque (B72y8). However, for the remaining cortical layers, the standardized cell numbers and the white matter interstitial cell numbers across the regions show a systematic decline with age. In addition, for the infragranular layers and WMICs, the data show that the highest cell numbers are at gyri, they are intermediate in numbers at linear regions, and lowest at sulci. Furthermore, the layer thicknesses (St or Tt) deter-

mined for layers 5, 6a, and 6b are thickest at gyral regions, intermediate in thickness at linear regions, and thinnest at sulcal regions (Figure 5a–c).

The systematic decline in WMIC numbers across the three regions, and the somewhat invariant standardized cell numbers of supragranular layers across the regions, has resulted in a systematic increase in the cell ratio per WMIC (Figure 7b; A–C). For the infragranular layer 6b, the results show a systematic decline in cell ratios across the three regions. For layers 5 and 6a, the results point to an invariant relationship where the cell ratios are approximately constant (layer 5: 5.1 ± 0.1 ; layer 6a: 2.8 ± 0.1). Statistical analyses across all three macaques and across all regions show that for layer 6a, there is a significant variation (ANOVA, $p < .01$) but across gyri and linear regions, it is nonsignificant (layer 6a: gyri 3.0 ± 0.1 ; linear 3.0 ± 0.2 ; $p > .9$). For layer 5, it is nonsignificant across the three macaques and across the three regions (ANOVA, $p > .12$). In confirmation of the results from section 47, the combined data across all regions and across all seven sections of the three macaques show that there are five cortical neurons of layer 5 for every WMIC.

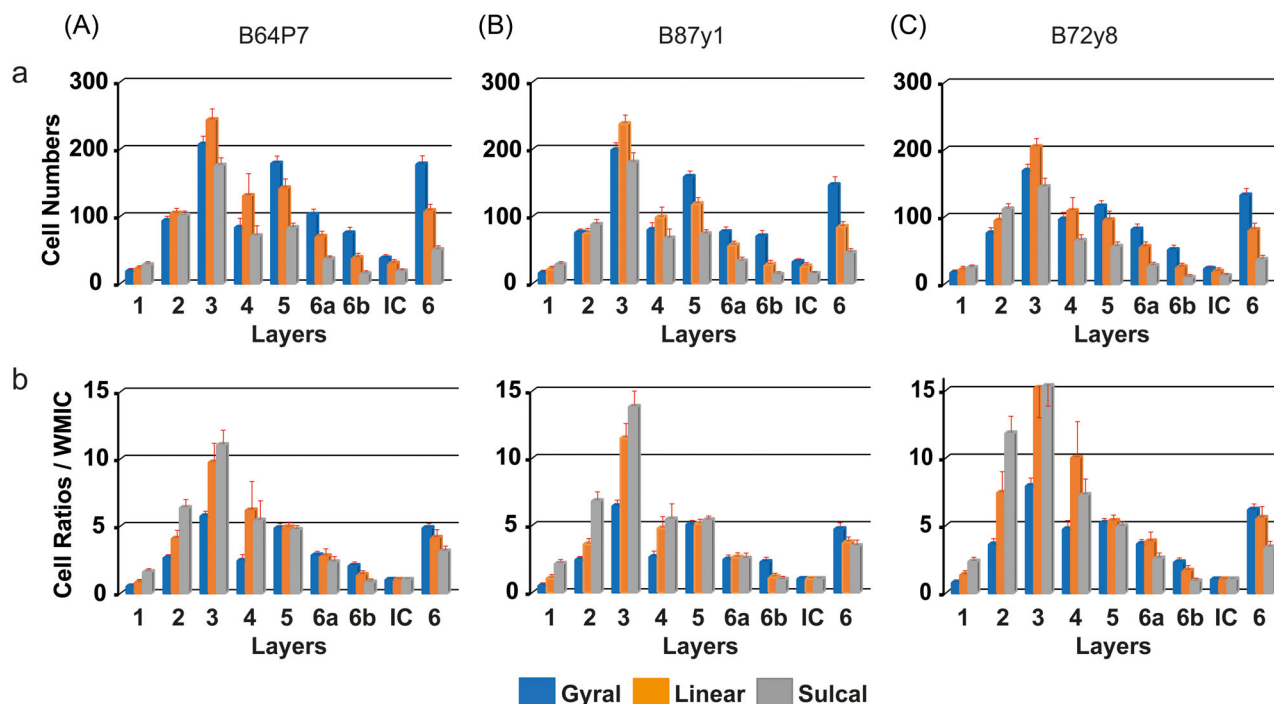


FIGURE 7 Analyses of standard cell numbers and cell numbers per white matter interstitial cell (WMIC) in cortical layers 1 to 6b and WMIC areas (IC), and combined histogram data for layers 6a and 6b as layer 6. Histogram data for all 7 sections from postnatal day 7, from 1.01-year-old and from 8.07-year-old macaques (A–C). The total numbers of gyri, linear regions, and sulci analyzed are given in Table 1. Top histograms (a) are for the standard cell numbers, and lower histograms (b) are the cell ratios per WMIC. Error bars ± 1 SEM.

4 | DISCUSSION

We have examined anteroposterior selected coronal sections immunolabelled with NeuN from three macaques. Our measurements, as in most previous publications, were performed in series of 2D sections rather than the 3D cerebral cortex and white matter with all the limitations of these approaches. Seven sections from each macaque, approximately 1 cm apart and ranging from anterior to posterior cortex, were analyzed at gyral, linear, and sulcal regions to determine their thicknesses (standard and tangential), and their standard cell numbers. This we carried out separately for each cortical layer. The layer boundaries were defined by visual inspection of the NeuN-labeled cell densities with the aid of adjacent Nissl-stained coronal sections. In addition, we calculated standard cell numbers at these same regions for interstitial cells from the underlying white matter below the layer 6b-white matter boundary. The layer 6b-white matter boundary was initially defined with the aid of the cell detection package QuPath which highlighted the fall in cell densities at the layer 6b-white matter boundary. This boundary was then visually inspected and refined to exclude clumps or strings of aligned pyramidal cells (details in Figure 2).

One of the issues in standardizing cell numbers was the variation of the thickness of cortical layers, especially at gyral and sulcal regions. For this, we used a protocol (Figure 3a) where we measured the layer thickness every 100 μ m from the dorsal layer boundary and then took the mean value. This allowed us to standardize cell numbers for the layer. Here we should note that before deciding on the 100 μ m length, in several cases, we measured thickness at separations along the dorsal

boundary of the layer at 25, 50, 100, 150, 200, and 300 μ m (Figure 4). We found that the 100 μ m separation gave us a value in reasonable agreement with those obtained at 25 and 50 μ m. In many cases (linear regions of cortex), the layer thicknesses were much more uniform over their length. For these, we took the layer thickness as the layer area divided by the mean of the dorsal and ventral boundaries (Figure 4). Again, these values were in close agreement with those determined at separations of 100 μ m (Figure 4c).

Our results of layer thicknesses show that supragranular layers at gyral and linear regions of cortex, excluding primary visual cortex, remain fairly uniform in thickness when calculated from our method of St or measured as Tt. In both cases, layer 1 at the sulcal locations substantially thickened (Figure 5, Table 3). For the infragranular layers, there was a systematic decline in thickness at all regions with layer 6b decreasing to a few cells thick at sulci. As a ratio of supragranular layers to infragranular layers: the St at gyri 1.2:1, at linear 2.0:1, at sulci 3.1:1; and the Tt at gyri 0.9:1, at linear 2.0:1, and at sulci 4.0:1. These results are in general agreement with those from the ferret (Horiuchi-Hirose & Sawada, 2016) and primate (Hilgetag & Barbas, 2006). The reasons behind variations in thickness are not clear, and several models or theories have been proposed. They include physical (Van Essen, 1997), biological (Cowan et al., 1984), and genetic (Baare et al., 2001; Rakic, 2004).

The developmental role of the subplate neurons is relatively better understood than the role of the remnant neurons in the adult (Molnár, 2019; Molnár & Kwan, 2024). Despite the disease association (Colombo, 2018; Kostović et al., 2011; Suárez-Solá et al.,

2009), the remnants of the subplate neurons in layer 6b in mouse and cortical interstitial white matter neurons in primates have not been integrated into models of intra- and extra-cortical adult circuits. Recent anatomical and physiological studies in rodent (Hoerder-Suabedissen et al., 2018; Zolnik et al., 2023) revealed circuits that could influence information transfer and brain state regulation. Chronic in vivo silencing of layer 6b neurons in mice reduces anxiety-related behavior (Guidi et al., 2016) and reduces sleep electroencephalogram spindle activity (Meijer et al., 2022). Our finding that the numbers of cortical WMICs correlate with cortical layer 5 neuron numbers fits with the theory that WMICs regulate cortical states (Kostovic et al., 2011; Molnár, 2019; Zolnik et al., 2023).

Our analyses show that densities of WMICs are highest at gyral Crowns, intermediate at linear regions, and lowest at sulci as it has been previously reported across primates by Swiegers et al. (2019, 2021) in gibbon, chimpanzee, squirrel monkey, and crested macaque. We also show that the thicknesses of layers 5, 6a, and 6b are thickest at gyral crowns, intermediate in linear regions, and thinnest at sulci. Previous studies have demonstrated strong correlation between the number of WMICs and the number of cortical neurons (Swiegers et al., 2019, 2021). Our study specifically establishes that this link is the strongest between the number of layer 5 neurons and WMICs. Moreover, we show that despite the regional variation of WMICs and infragranular layers, there are five cortical neurons from layer 5 for each interstitial neuron and possibly three cortical neurons from layer 6a for each interstitial cell irrespective whether the interstitial neurons are located within the white matter below gyri, linear, or sulci regions. It is known that interstitial neurons make reciprocal connections with cortical layers 5 and 6 (Hanganu et al., 2002; Zolnik et al., 2023). The similarities in gene expression between layer 5 and subplate-derived layer 6b in the mouse have been emphasized by previous studies (Belgard et al., 2011; Hoerder-Suabedissen et al., 2013). The constant ratio between WMICs and layer 5 neurons, despite the areal variation of the cell numbers in gyri, linear, or sulci regions, indicates a possible scaling of cell numbers between these neurons within these areas. This scaling might occur during neurogenesis, or during the preferential cell death of interstitial neurons. It is not yet clear whether the WMICs are dependent on the density of neurons within layers 5 and 6a, or the other way around, that is, subplate and WMIC numbers regulate infragranular cell numbers. Change in density and distribution of interstitial neurons has been observed in schizophrenia and epilepsy (Akbarian et al., 1996; Anderson et al., 1996; Eastwood & Harrison, 2003; Fung et al., 2014; Kirkpatrick et al., 1999, 2003; Meencke, 1983; Richter et al., 2016). It will require further studies to explore whether the altered distribution and cell numbers of WMICs that is observed in these conditions may be associated with alterations in respective cell numbers in layers 5 and 6a and whether the modifications in neuronal numbers are causally related.

ACKNOWLEDGMENTS

NIH Grant MH113257 (to AD). The work in ZM's laboratory is funded by BBSRC Project Grant BB/X008711/1; MRC Project Grant

MR/W029073/1 and Einstein Stiftung Berlin as part of ZM being Einstein Fellow at Charité Universitätsmedizin Berlin.

CONFLICT OF INTEREST STATEMENT

The authors declare no conflicts of interest.

DATA AVAILABILITY STATEMENT

Our article is based on publicly available materials in Collection 6 of the MacBrain Resource Center hosted in the Department of Neuroscience at Yale University School of Medicine (<https://medicine.yale.edu/neuroscience/macbrain/>).

ORCID

Bashir Ahmed  <https://orcid.org/0000-0001-9989-2659>

Zoltán Molnár  <https://orcid.org/0000-0002-6852-6004>

PEER REVIEW

The peer review history for this article is available at <https://publons.com/publon/10.1002/cne.25626>.

REFERENCES

- Akbarian, S., Kim, J. J., Potkin, S. G., Hetrick, W. P., Bunney, W. E., Jr., & Jones, E. G. (1996). Maldistribution of interstitial neurons in prefrontal white matter of the brains of schizophrenic patients. *Archives of General Psychiatry*, 53, 425–436.
- Anderson, S. A., Volk, D. W., & Lewis, D. A. (1996). Increased density of microtubule associated protein 2-immunoreactive neurons in the prefrontal white matter of schizophrenic subjects. *Schizophrenia Research*, 19, 111–119.
- Baare, W. F., Hulshoff Pol, H. E., Boomsma, D. I., Posthuma, D., de Geus, E. J., Schnack, H. G., van Haren, N. E., van Oel, C. J., & Kahn, R. S. (2001). Quantitative genetic modeling of variation in human brain morphology. *Cerebral Cortex*, 11, 816–824.
- Belgard, T. G., Marques, A. C., Oliver, P. L., Abaan, H. O., Sirey, T. M., Hoerder-Suabedissen, A., García-Moreno, F., Molnár, Z., Margulies, E. H., & Ponting, C. P. (2011). Transcriptomic atlas of mouse neocortical layers. *Neuron*, 7, 605–616.
- Berman, N. E. J., & Fredrickson, E. (1992). Morphology and laminar distribution of neuropeptide Y immunoreactive neurons in the human striate cortex. *Synapse*, 11, 20–27.
- Brodmann, K. (1914). Physiologie des Gehirns. Die anatomische Feldertopographie der Grosshirnoberfläche. In F. Krause (Ed.), *Die Allgemeine Chirurgie der Gehirnkrankheiten* (pp. 99–112). Ferdinand Enke.
- Bankhead, P., Loughrey, M. B., Fernández, J. A., Dombrowski, Y., McArt, D. G., Dunne, P. D., McQuaid, S., Gray, R. T., Murray, R. T., Coleman, H. G., James, J. A., Salto-Tellez, M., & Hamilton, P. W. (2017). QuPath: Open source software for digital pathology image analysis. *Scientific Reports*, 7, 16878.
- Chan-Palay, V., Allen, Y. S., Lang, W., Haesler, U., & Polak, J. M. I. (1985). Cytology and distribution in normal human cerebral cortex of neurons immunoreactive with antisera against neuropeptide Y. *Journal of Comparative Neurology*, 238, 382–389.
- Chun, J. J. M., & Shatz, C. J. (1989). Interstitial cells of the adult neocortical white matter are the remnant of the early generated subplate neuron population. *Journal of Comparative Neurology*, 282, 555–569.
- Clancy, B., & Cauller, L. J. (1999). Widespread projections from subgriseal neurons (layer VII) to layer I in adult rat cortex. *Journal of Comparative Neurology*, 407, 275–286.
- Clancy, B., Silva-Filho, M., & Friedlander, M. J. (2001). Structure and projections of white matter neurons in the postnatal rat visual cortex. *Journal of Comparative Neurology*, 434, 233–252.

- Colombo, J. A. (2018). Cellular complexity in subcortical white matter: A distributed control circuit? *Brain Structure & Function*, 223, 981–985.
- Cowan, W. M., Fawcett, J. W., O'Leary, D. D., & Stanfield, B. B. (1984). Regressive events in neurogenesis. *Science*, 225, 1258–1265.
- Das, G. D., & Kreutzberg, G. W. (1968). Evaluation of interstitial nerve cells in the central nervous system: A correlative study using acetylcholinesterase and Golgi techniques. *Ergebnisse der Anatomie und Entwicklungsgeschichte*, 41, 1–58.
- Duque, A., Gazula, V. R., & Kaczmarek, L. K. (2013). Expression of Kv1.3 potassium channels regulates density of cortical interneurons. *Developmental Neurobiology*, 73, 841–855.
- Duque, A., Krsnik, Z., Kostović, I., & Rakic, P. (2016). Secondary expansion of the transient subplate zone in the developing cerebrum of human and nonhuman primates. *PNAS*, 113, 9892–9897.
- Duque, A., Tepper, J. M., Detari, L., Ascoli, G. A., & Zaborszky, L. (2007). Morphological characterization of electrophysiologically and immunohistochemically identified basal forebrain cholinergic and neuropeptide Y-containing neurons. *Brain Structure & Function*, 212, 55–73.
- Eastwood, S. L., & Harrison, P. J. (2003). Interstitial white matter neurons express less reelin and are abnormally distributed in schizophrenia: Towards an integration of molecular and morphologic aspects of the neurodevelopmental hypothesis. *Molecular Psychiatry*, 769, 821–831.
- Eastwood, S. L., & Harrison, P. J. (2005). Interstitial white matter neuron density in the dorsolateral prefrontal cortex and parahippocampal gyrus in schizophrenia. *Schizophrenia Research*, 79, 181–188.
- Feldmeyer, D. (2023). Structure and function of neocortical layer 6b. *Frontiers in Cellular Neuroscience*, 17, 1257803.
- Fischer, H. C., & Kuljis, R. O. (1994). Multiple types of nitrogen monoxide synthase-/NADPH diaphorase-containing neurons in the human cerebral neocortex. *Brain Research*, 654, 105–117.
- Friauf, E., McConnell, S. K., & Shatz, C. J. (1990). Functional synaptic circuits in the subplate during fetal and early postnatal development of cat visual cortex. *Journal of Neuroscience*, 10, 2601–2613. <https://doi.org/10.1523/JNEUROSCI.10-08-02601>
- Friauf, E., & Shatz, C. J. (1991). Changing patterns of synaptic input to subplate and cortical plate during development of visual cortex. *Journal of Neurophysiology*, 66, 2059–2071.
- Fung, S. J., Joshi, D., Fillman, S. G., & Weickert, C. S. (2014). High white matter neuron density with elevated cortical cytokine expression in schizophrenia. *Biological Psychiatry*, 75, 5–7.
- Garcia-Marin, V., Blazquez-Llorca, L., Rodriguez, J. R., Gonzalez-Soriano, J., & DeFelipe, J. (2010). Differential distribution of neurons in the gyral white matter of the human cerebral cortex. *Journal of Comparative Neurology*, 518, 4740–4759.
- Ghosh, A., Antonini, A., McConnell, S. K., & Shatz, C. J. (1990). Requirement for subplate neurons in the formation of thalamocortical connections. *Nature*, 347, 179–181.
- Guidi, L., Korrell, K. V., Hoerder-Suabedissen, A., Oliver, P. L., Wilson, M. C., Kanold, P. O., Bannerman, D., & Molnár, Z. (2016). Functional role of cortical layer VIb in mouse behaviour. *SFN Abstracts*, 634, 16.
- Hanganu, I. L., Kilb, W., & Luhmann, H. J. (2002). Functional synaptic projections onto subplate neurons in neonatal rat somatosensory cortex. *Journal of Neuroscience*, 22, 7165–7176.
- Higashi, S., Hioki, K., Kurotani, T., Kasim, N., & Molnár, Z. (2005). Functional thalamocortical synapse reorganization from subplate to layer IV during postnatal development in the reeler-like mutant rat (Shaking Rat Kawasaki). *Journal of Neuroscience*, 25, 1395–1406. <https://doi.org/10.1523/JNEUROSCI.4023-04.2005>
- Higashi, S., Molnár, Z., Kurotani, T., & Toyama, K. (2002). Prenatal development of neural excitation in rat thalamocortical preparations studied by optical recording. *Neuroscience*, 115, 1231–1246.
- Hilgetag, C. C., & Barbas, H. (2006). Role of mechanical factors in the morphology of the primate cerebral cortex. *PLOS Computational Biology*, 2, 146–159.
- Hoerder-Suabedissen, A., Hayashi, S., Upton, L., Nolan, Z., Casas-Torremocha, D., Grant, E., Viswanathan, S., Kanold, P. O., Clasca, F., Kim, Y., & Molnár, Z. (2018). Subset of cortical layer 6b neurons selectively innervate higher order thalamic nuclei in mice. *Cerebral Cortex*, 28, 1882–1897.
- Hoerder-Suabedissen, A., Oeschger, F. M., Krishnan, M. L., Belgard, T. G., Wang, W. Z., Lee, S., Webber, C., Petretto, E., Edwards, A. D., & Molnár, Z. (2013). Expression profiling of mouse subplate reveals a dynamic gene network and disease association with autism and schizophrenia. *PNAS*, 110, 3555–3560.
- Horiuchi-Hirose, M., & Sawada, K. (2016). Differential cortical laminar structure revealed by NeuN immunostaining and myeloarchitecture between sulcal and gyral regions independent of sexual dimorphisms in the ferret cerebrum. *Anatomical Record*, 299, 1003–1011.
- Juan, F., Montiel, J. F., Wang, W. Z., Oeschger, F. M., Hoerder-Suabedissen, A., Tung, W. L., García-Moreno, F., Holm, I. E., Villalón, A., & Molnár, Z. (2011). Hypothesis on the dual origin of the mammalian subplate. *Frontiers in Neuroanatomy*, 5(25), 1–10.
- Judaš, M., Sedmak, G., Pletikos, M., & Jovanov-Milošević, N. (2010). Population of subplate and interstitial neurons in fetal and adult human telencephalon. *Journal of Anatomy*, 217, 381–399.
- Judaš, M., Šestan, N., & Kostovic, I. (1999). Nitrinergic neurons in the developing and adult human telencephalon: Transient and permanent patterns of expression in comparison to other mammals. *Microscopy Research and Technique*, 45, 401–419.
- Kanold, P. O., & Luhmann, H. J. (2010). The subplate and early cortical circuits. *Annual Review of Neuroscience*, 33, 23–48.
- Kanold, P. O., & Shatz, C. J. (2006). Subplate neurons regulate maturation of cortical inhibition and outcome of ocular dominance plasticity. *Neuron*, 51, 627–638.
- Kilduff, T. S., Cauli, B., & Gerashchenko, D. (2011). Activation of cortical interneurons during sleep: An anatomical link to homeostatic sleep regulation. *Trends in Neuroscience (Tins)*, 34, 10–19.
- Kirkpatrick, B., Conley, R. C., Kakoyannis, A., Reep, R. L., & Roberts, R. C. (1999). Interstitial cells of the white matter in the inferior parietal cortex in schizophrenia: An unbiased cell-counting study. *Synapse*, 34, 95–102.
- Kirkpatrick, B., Messias, N. C., Conley, R. R., & Roberts, R. C. (2003). Interstitial cells of the white matter in the dorsolateral prefrontal cortex in deficit and nondeficit schizophrenia. *Journal of Nervous and Mental Disease*, 191, 563–567.
- Kostović, I., Jovanov-Milošević, N., Radoš, M., Sedmak, G., Benjak, V., Kostović-Srzić, M., Vasung, L., Čuljat, M., Radoš, M., Hüppi, P., & Judaš, M. (2014). Perinatal and early postnatal reorganization of the subplate and related cellular compartments in the human cerebral wall as revealed by histological and MRI approaches. *Brain Structure & Function*, 219, 231–253.
- Kostović, I., Judaš, M., & Sedmak, G. (2011). Developmental history of the subplate zone, subplate neurons and interstitial white matter neurons: Relevance for schizophrenia. *International Journal of Developmental Neuroscience*, 29, 193–205.
- Kostović, I., & Molliver, M. E. (1974). New interpretation of laminar development of cerebral-cortex-synaptogenesis in different layers of neopallium in human fetus. *Anatomical Record*, 178, 395.
- Kostović, I., Molliver, M. E., & Van der Loos, H. (1973). The laminar distribution of synapses in neocortex of fetal dog. *Anatomical Record*, 175, 362.
- Kostović, I., & Rakic, P. (1980). Cytology and time of origin of interstitial neurons in the white matter in infant and adult human and monkey telencephalon. *Journal of Neurocytology*, 9, 219–242.
- Kostović, I., & Rakic, P. (1990). Developmental history of the transient subplate zone in visual and somatosensory cortex of the macaque monkey and human brain. *Journal of Comparative Neurology*, 297, 441–470.
- Kostović, I., Štefulj-Fucic, A., Mrzljak, L., Jukic, S., & Delalle, I. (1991). Prenatal and perinatal development of the somatostatin immunoreactive neurons in the human prefrontal cortex. *Neuroscience Letters*, 124, 153–156.
- Lopez-Bendito, G., & Molnar, Z. (2003). Thalamocortical development: How are we going to get there? *Nature Reviews Neuroscience*, 4, 276–289.

- Marín-Padilla, M. (1971). Early prenatal ontogenesis of the cerebral cortex (neocortex) of the cat (*Felis domestica*). A Golgi study. I. The primordial neocortical organization. *Zeitschrift für Anatomie und Entwicklungsgeschichte*, 134, 117–1145.
- Meencke, H. J. (1983). The density of dystopic neurons in the white matter of the *Gyrus frontalis* in epilepsies. *Journal of Neurology*, 230, 171–181.
- Meijer, E. J., Krone, L. B., Mengual, J. P., Hoerder-Suabedissen, A., Yamagata, T., Vyazovskiy, V. V., & Molnár, Z. (2022). A reduction in sleep EEG spindle activity in “layer 6b silenced” mice. *SFN Abstracts*, 223, 03.
- Meyer, G., Gonzales-Hernandez, T., Galindo-Mireles, D., Castaneyra-Perdomo, A., & Ferres-Torres, R. (1991). The efferent projections of neurons in the white matter of different cortical areas of the adult rat. *Anatomy and Embryology*, 184, 99–102.
- Meyer, G., Wahle, P., Castaneyra-Perdomo, A., & Ferres-Torres, R. (1992). Morphology of neurons in the white matter of the adult human neocortex. *Experimental Brain Research*, 88, 204–212.
- Molliver, M. E., & Van der Loos, H. (1970). The ontogenesis of cortical circuitry: The spatial distribution of synapses in somesthetic cortex of newborn dog. *Ergebnisse der Anatomie und Entwicklungsgeschichte*, 42, 1–53.
- Molnár, Z. (2019). Cortical layer with no known function. *European Journal of Neuroscience*, 49, 957–963.
- Molnár, Z., Kurotani, T., Higashi, S., Yamamoto, N., & Toyama, K. (2003). Development of functional thalamocortical synapses studied with current source-density analysis in whole forebrain slices in the rat. *Brain Research Bulletin*, 60, 355–371.
- Molnár, Z., & Kwan, K. Y. (2024). Development and Evolution of Thalamocortical Connectivity. Cold Spring Harbor Perspectives in Biology, 16:a041503.
- Montiel, J. F., Wang, W. Z., Oeschger, F. M., Hoerder-Suabedissen, A., Tung, W. L., García-Moreno, F., Holm, I. E., Villalón, A., & Molnár, Z. (2011). Hypothesis on the dual origin of the Mammalian subplate. *Frontiers Neuroanatomy*, 7, 5–25.
- Mortazavi, F., Romano, S. E., Rosene, D. L., & Rockland, K. S. (2017). A survey of white matter neurons at the gyral crowns and sulcal depths in the Rhesus monkey. *Frontiers in Neuroanatomy*, 11, 69.
- Mortazavi, F., Wang, X. Y., Rosene, D. L., & Rockland, K. S. (2016). White matter neurons in young adult and aged rhesus monkey. *Frontiers in Neuroanatomy*, 10, 15.
- Okhotin, V. E., & Kalinichenko, S. G. (2003). Subcortical white matter interstitial cells: Their connections, neurochemical specialization, and role in the histogenesis of the cortex. *Neuroscience and Behavioral Physiology*, 33, 177–194.
- Rakic, P. (2004). Genetic control of cortical convolutions. *Science*, 303, 1983–1984.
- Rash, B. G., Duque, A., Morozova, Y. M., Arellano, J. I., Micalia, N., & Rakic, P. (2019). Gliogenesis in the outer subventricular zone promotes enlargement and gyrification of the primate cerebrum. *PNAS*, 116, 7089–7094.
- Richter, Z., Janszky, J., Setalo, G., Horvath, R., Horvath, Z., Dóczi, T., Seress, L., & Ábrahám, H. (2016). Characterization of neurons in the cortical white matter in human temporal lobe epilepsy. *Neuroscience*, 333, 140–150.
- Rojiani, A. M., Emery, J. A., Anderson, K. J., & Massey, J. K. (1996). Distribution of heterotopic neurons in normal hemispheric white matter: A morphometric analysis. *Journal of Neuropathology and Experimental Neurology*, 55, 178–183.
- Regidor, J., Edvinsson, L., & Divac, I. (1993). NOS neurones lie near branchings of cortical arterioles. *Neuroreport*, 4, 112–114.
- Sachs, H. (1892). *Das Hemisphaerenmark des menschlichen Grosshirns. I. Der Hinterhauptlappen*. Georg Thieme Verlag.
- Sedmak, G., & Judoš, M. (2019). The total number of white matter interstitial neurons in the human brain. *Journal of Anatomy*, 235, 626–636.
- Sedmak, G., & Judoš, M. (2021). White matter interstitial neurons in the adult human brain: 3% of cortical neurons in quest for recognition. *Cells*, 10, 190–202.
- Shering, A. F., & Lowenstein, P. R. (1994). Neocortex provides direct synaptic input to interstitial neurons of the intermediate zone of kittens and white matter of cats: A light and electron microscopy study. *Journal of Comparative Neurology*, 347, 433–443.
- Smiley, J. F., Levey, A. I., & Mesulam, M. M. (1998). Infracortical interstitial cells concurrently express m2-muscarinic receptors, acetylcholinesterase and nicotinamide adenine dinucleotide phosphate-diaphorase in the human and monkey cerebral cortex. *Neuroscience*, 84, 755–769.
- Suárez-Solá, M. L., González-Delgado, F. J., Pueyo-Morlans, M., Medina-Bolívar, O. C., Hernández-Acosta, N. C., Gonzalez-Gomez, M., & Meyer, G. (2009). Neurons in the white matter of the adult human neocortex. *Frontiers in Neuroanatomy*, 3(7), 1–7.
- Swiegers, J., Bhagwandin, A., Sherwood, C. C., Bertelsen, M. F., Maseko, B. C., Hemingway, J., Rockland, K. S., Molnár, Z., & Anger, P. R. (2019). The distribution, number, and certain neurochemical identities of infracortical white matter neurons in a lar gibbon (*Hylobates lar*) brain. *Journal of Comparative Neurology*, 527, 1633–1653.
- Swiegers, J., Bhagwandin, A., Williams, V. M., Maseko, B. C., Sherwood, C. C., Hård, T., Bertelsen, M. F., Rockland, K. S., Molnár, Z., & Manger, P. R. (2021). The distribution, number, and certain neurochemical identities of infracortical white matter neurons in a chimpanzee (*Pan troglodytes*) brain. *Journal of Comparative Neurology*, 529, 3429–3452.
- Torres-Reveron, J., & Friedlander, M. J. (2007). Properties of persistent postnatal cortical subplate neurons. *Journal of Neuroscience*, 27, 9962–9974.
- Uyilings, H. B. M., & Delalle, I. (1997). Morphology of neuropeptide Y-immunoreactive neurons and fibers in human prefrontal cortex during prenatal and postnatal development. *Journal of Comparative Neurology*, 379, 523–540.
- Valverde, F., & Facal-Valverde, M. V. (1988). Postnatal development of interstitial (subplate) cells in the white matter of the temporal cortex of kittens: A correlated Golgi and electron microscopy study. *Journal of Comparative Neurology*, 269, 168–192.
- Van Essen, D. C. (1997). A tension-based theory of morphogenesis and compact wiring in the central nervous system. *Nature*, 385, 313–318.
- Viswanathan, S., Sheikh, A., Looger, L. L., & Kanold, P. O. (2017). Molecularly defined subplate neurons project both to thalamocortical recipient layers and thalamus. *Cerebral Cortex*, 27, 4759–4768.
- Von Monakow, C. (1905). *Gehirnpathologie*. Alfred Holder.
- Wang, W. Z., Oeschger, F. M., Montiel, J. F., García-Moreno, F., Hoerder-Suabedissen, A., Krubitzer, L., Ek, C. J., Saunders, N. R., Reim, K., Villalón, A., & Molnár, Z. (2011). Comparative aspects of subplate zone studied with gene expression in sauropsids and mammals. *Cerebral Cortex*, 21, 2187–2203.
- Zolnik, T. A., Bronec, A., Ross, A., Molnár, Z., Eickholt, B. J., & Larkum, M. E. (2023). Layer 6b controls brain state via apical dendrites and the higher-order thalamocortical system. *Neuron*, 14, 2023. <https://doi.org/10.1016/j.neuron.2023.11.021>
- Žunić Išasegi, I., Radoš, M., Krsnik, Ž., Radoš, M., Benjak, V., & Kostović, I. (2018). Interactive histogenesis of axonal strata and proliferative zones in the human fetal cerebral wall. *Brain Structure & Function*, 223, 3919–3943.

How to cite this article: Ahmed, B., Duque, A., Rakic, P., & Molnár, Z. (2024). Correlation between the number of interstitial neurons of the white matter and number of neurons within cortical layers: Histological analyses in postnatal macaque. *Journal of Comparative Neurology*, 532, e25626. <https://doi.org/10.1002/cne.25626>